PROCEEDINGS OF SPIE

SPIEDigitalLibrary.org/conference-proceedings-of-spie

Modeling electroelastic nonlinearities in ultrasound acoustic energy transfer systems

Vamsi C. Meesala, Muhammad R. Hajj, Shima Shahab

Vamsi C. Meesala, Muhammad R. Hajj, Shima Shahab, "Modeling electroelastic nonlinearities in ultrasound acoustic energy transfer systems," Proc. SPIE 10595, Active and Passive Smart Structures and Integrated Systems XII, 105951G (16 March 2018); doi: 10.1117/12.2300858

SPIE.

Event: SPIE Smart Structures and Materials + Nondestructive Evaluation and Health Monitoring, 2018, Denver, Colorado, United States

Downloaded From: https://www.spiedigitallibrary.org/conference-proceedings-of-spie on 7/17/2018 Terms of Use: https://www.spiedigitallibrary.org/terms-of-use

Modeling Electroelastic Nonlinearities in Ultrasound Acoustic Energy Transfer Systems

Vamsi C. Meesala, Muhammad R. Hajj and Shima Shahab

Department of Biomedical Engineering and Mechanics, Virginia Tech, Blacksburg, VA, USA

ABSTRACT

Ultrasound acoustic energy transfer systems are receiving growing attention in the area of contactless energy transfer for its advantages over other approaches, such as inductive coupling method. To date, most research on this approach has been on modeling and proof-of-concept experiments in the linear regime where nonlinear effects associated with high excitation levels are not significant. We present an acoustic-electroelastic model of a piezoelectric receiver in water by considering its nonlinear constitutive relations. The theory is based on ideal spherical sound wave propagation in conjunction with the electroelastic distributed-parameter governing equations for the receiver's vibration and the electrical circuit.

Keywords: Ultrasound acoustic energy transfer, Contactless energy transfer, Smart materials, Method of Multiple Scales, Nonlinear strains, Softening nonlinearity, Optimum Resistance

1. INTRODUCTION

Ultrasound Acoustic Energy Transfer (UAET) systems are receiving growing attention in the area of contactless energy transfer for its advantages over otherwise familiar and well-studied methods, such as the inductive coupling method. UAET can contribute to the development, use, and reliability of low-power sensors, control devices and communication networks in applications where wired electrical contact is dangerous or impractical. A thorough literature review on UAET and its advantages over inductive, microwave, capacitive, and optical energy transfer methods is presented by Roes et al.[1] The limited research till now has been on modeling and proof-of-concept experiments in the linear regime, suggesting that the amount of energy transferred will increase proportionally to the increase in excitation amplitude. Shahab et al.,[2] Shahab and Erturk[3] pioneered the early efforts on developing a fully-coupled mathematical model for the multi-physics problem. They considered an incident acoustic wave, originating from a source of known strength and developed a model to analyze the electrical power output extracted by a free-free piezoelectric (PZT) receiver and validated with FEM simulations. Shahab et al.[4,5] later experimentally validated the theoretical framework.

The linear analysis will fail as the amplitude of elastic strains in the receiver induced by the acoustic waves becomes significant and when those strains couple nonlinearly with the electric field generated by the receiver. Under these conditions, there is a need to solve the coupled problem by accounting for both acoustic nonlinearities of the medium and the nonlinear electroelastic response of the PZT receiver. As a first step to tackle this challenge, we present an acoustic-electroelastic model of a PZT receiver that takes its nonlinear constitutive relations into consideration. Since the goal is to study the effect of nonlinear strains, we consider the enthalpy proposed by Wagner and Hagedorn,[6] which is developed by approximating Young's modulus and piezoelectric coupling coefficients with higher order strains. We neglect the attenuation and transfer of energy to higher frequencies in sound signal due to its propagation in the fluid medium. Assuming an acoustic excitation from an ideal spherical source, we develop distributed-parameter governing equations of the receiver's vibration and the electrical circuit. The mathematical framework can be used for optimized design fabrication and testing of UAET prototypes over a broad range of scales targeting different industrial and biomedical applications.

Send correspondence to Vamsi, E-mail: vamsi24@vt.edu, Telephone: 1 361 406 7560

Active and Passive Smart Structures and Integrated Systems XII, edited by Alper Erturk, Jae-Hung Han,
Proc. of SPIE Vol. 10595, 105951G · © 2018 SPIE · CCC code: 0277-786X/18/$18 · doi: 10.1117/12.2300858

Downloaded From: https://www.spiedigitallibrary.org/conference-proceedings-of-spie on 7/17/2018
Terms of Use: https://www.spiedigitallibrary.org/terms-of-use

2. MATHEMATICAL MODELING

A piezoelectric disk of thickness l and radius r is chosen as the receiver and is subjected to an acoustic excitation from a spherical source, as shown in figure 1. We derive the governing equations of the PZT disk using extended Hamilton's principle for electronic transducer written as[6–9] :

$$\int_{t_1}^{t_2} \delta(T - \Pi + W_e + W)\, dt \equiv \int_{t_1}^{t_2} \delta(T - \Delta + W)\, dt = 0 \tag{1}$$

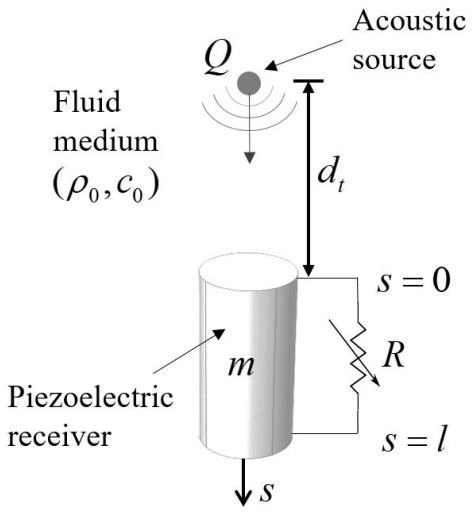

Figure 1. Schematic of the piezoelectric receiver.

We define a co-ordinate, s along the axis of the disk (Ox_3) and identify the flat surfaces as $s = 0$ and $s = l$ as shown in figure 1. Defining $u(s,t)$ as the displacement at any time t of the material located at s, we write the kinetic energy as,

$$T = \frac{1}{2}\int_0^l m\dot{u}(s,t)^2\, ds \tag{2}$$

where m is mass per unit length of the receiver.

To account for the effects of large (nonlinear) strains, we use the electric enthalpy derived by Wagner and Hagedorn[6] as:

$$\Delta = \int_0^l A\left(\frac{1}{2}Y_{33}\varepsilon_{33}^2 - e_{33}\varepsilon_{33}E_3 - \frac{1}{2}\alpha_3 E_3\varepsilon_{33}^2 - \frac{1}{2}\epsilon_{33}^S E_3^2 + \frac{1}{6}\alpha_1\varepsilon_{33}^3 - \frac{1}{6}\alpha_2\varepsilon_{33}^3 E_3 + \frac{1}{8}\alpha_4\varepsilon_{33}^4\right) ds \tag{3}$$

where Y_{33}, e_{33}, ε_{33}^S and A are respectively the elastic modulus (thickness mode Young's modulus), piezoelectric coupling co-efficient, dielectric (or piezoelectric permittivity) constant and cross-sectional area of the disk,and α_1, α_2, α_3 and α_4 are parameters that govern the nonlinearity in the system. The induced electric field due to the strain generated inside the cylinder in 3−direction is denoted by $E_3(s,t)$ and can be related to generated electric potential by,

$$E_3(s,t) = -\frac{V_H(s,t)}{l} \tag{4}$$

where

$$V_H(s,t) = V(t)\left[H(s) - H(s-l)\right], \tag{5a}$$

$$V_H(s,t)^n = V(t)^n\left[H(s) - H(s-l)\right] \tag{5b}$$

Downloaded From: https://www.spiedigitallibrary.org/conference-proceedings-of-spie on 7/17/2018
Terms of Use: https://www.spiedigitallibrary.org/terms-of-use

and $H(s)$ is the heaviside function.

Assuming that the acoustic excitation is generated by a point (spherical) source ($ka_{source} << 1$), such as NH0040 needle hydrophone by precision acoustics, the pressure on the top surface of the disk is given by

$$p_t(t) \approx j\rho_0 c_0 k \frac{Q}{4\pi}\frac{1}{d_t}e^{j(\omega t - kd_t)} = j\rho_0\omega\frac{Q}{4\pi}\frac{1}{d_t}e^{j(\omega t - kd_t)} \tag{6}$$

where ρ_0, c_0, ω, Q and d_t are respectively the density of the medium, velocity of sound in medium, excitation frequency, source strength and distance from source to the top surface of the disk.

By placing the disk in a dense medium, the vibrations of its surfaces generate their own pressure fields that would interfere with the excitation. We account for this effect by introducing a radiation impedance, Z_r, that represents the reaction forces induced in the medium as a result of the motion of the disk's surfaces. For a circular disk with infinite baffle, this impedance is defined as.[10]

$$Z_r = R_r + jX_r = -\frac{F_r}{\dot{u}} = \frac{1}{\dot{u}}\iint_S p(\vec{r})\,dS \tag{7a}$$

where R_r and X_r represent respectively the self radiation resistance and reactance. The average value of of Z_r for a circular piston in an infinite baffle was derived by Butler and Sherman[10] and is given by

$$Z_r = \rho_0 c_0 A\left[1 - \frac{J_1(2ka)}{ka} + j\frac{S_1(2ka)}{ka}\right] \tag{7b}$$

where J_1 and S_1 represent respectively the first order Bessel and Struve functions, and ρ_0 and c_0 represent respectively the density and velocity of the sound in medium.

The variational work by non conservative forces - structural damping, acoustic excitation and radiation impedance - is given by

$$\delta W = f_t(t)\delta u(0,t) - f_b(t-\tau)\delta u(l,t) - \int_0^l c_s\dot{u}(s,t)\delta u(s,t)\,ds \\ - Z_r\dot{u}(0,t)\delta u(0,t) - Z_r\dot{u}(l,t)\delta u(l,t) - Q\delta V \tag{8a}$$

where

$$f_t(t) \approx p_t A = p_t\pi a_r^2, \qquad f_b(t-\tau) \approx p_b\pi a_r^2, \tag{8b}$$

$$p_b(t) = j\rho_0 c_0 k\frac{Q}{4\pi}\frac{1}{d_b}e^{j(\omega t - kd_b)} = \chi p_t e^{-j\omega\tau}, \qquad \chi = \frac{d_t}{d_b}, \text{ and } \quad \tau = \frac{k(d_b - d_t)}{\omega}, \tag{8c}$$

Here c_s is structural damping, a_r is the radius of receiver and p_t and p_b are respectively the acoustic pressures on the top and bottom surfaces of the disk which are assumed to be uniformly distributed over its cross-sectional area. The negative sign for the force is the consequence of direction of f_b being in the negative s direction. Substituting equations. 2, 3 and 8a into equation 1, the full nonlinear governing equations are derived as:

$$-m\ddot{u} + Y_{33}Au'' + e_{33}A\frac{V'}{l} + \alpha_3 A\left(\frac{V}{l}u'' + \frac{V'}{l}u'\right) + \alpha_1 Au'u'' + \frac{1}{2}\alpha_2 A\left(u'^2\frac{V'}{l} + 2u'u''\frac{V}{l}\right) \\ + \frac{3}{2}\alpha_4 Au'^2u'' - c_s\dot{u} + f_t\delta[s] - f_b\delta[s-l] - R_r\dot{u}\delta[s] - R_r\dot{u}\delta[s-l] = 0 \tag{9}$$

$$\int_0^l\left[-\frac{1}{2}\alpha_3 A\frac{1}{l}u'^2 - e_{33}Au'\frac{1}{l} + \epsilon_{33}^S A\frac{V}{l^2} - \frac{1}{6}\alpha_2 Au'^3\frac{1}{l}\right]ds - Q = 0 \tag{10}$$

with the boundary conditions,

$$-m_r\ddot{u} + Y_{33}Au' + e_{33}A\frac{V}{l} + \alpha_3 A\frac{V}{l}u' + \frac{1}{2}\alpha_1 Au'^2 + \frac{1}{2}\alpha_2 Au'^2\frac{V}{l} + \frac{1}{2}\alpha_4 Au'^3\Big|_{s=0} = 0 \tag{11}$$

Downloaded From: https://www.spiedigitallibrary.org/conference-proceedings-of-spie on 7/17/2018
Terms of Use: https://www.spiedigitallibrary.org/terms-of-use

$$-m_r\ddot{u} - Y_{33}Au' - e_{33}A\frac{V}{l} - \alpha_3 A\frac{V}{l}u' - \frac{1}{2}\alpha_1 Au'^2 - \frac{1}{2}\alpha_2 Au'^2\frac{V}{l} - \frac{1}{2}\alpha_4 Au'^3\Big|_{s=l} = 0 \tag{12}$$

where m_r is the radiation mass and is given by $m = X_r/\omega$.

Implementing the Galerkin's discretization, $u(s,t) = \sum_{i=1}^{n}\phi_i(s)q_i(t)$ and using the weighted residual method, we determine the governing equations of the temporal modes, q_j. To this end, we substitute the discretization and multiply equation 9 by the linear mode shape, $\phi_j(s)$ and integrate it over the thickness of structure. Using the normalization and nonlinear boundary conditions, we obtain the governing equation of k^{th} mode or actuation equation as

$$\ddot{q}_k + \omega_k^2 q_k + \sum_{i=1}^{n}\dot{q}_i\left[\int_0^l c_s\phi_k\phi_i\,ds + R_r\phi_i\phi_k|_{s=0} + R_r\phi_i\phi_k|_{s=l}\right] + \int_0^l \phi_k' e_{33}A\frac{V_H}{l}\,ds$$
$$+ \sum_{i=1}^{n} q_i\int_0^l \alpha_3 A\phi_k'\phi_i'\frac{V_H}{l}\,ds + \frac{1}{2}\sum_{i=1}^{n}\sum_{j=1}^{n} q_iq_j\int_0^l \alpha_1 A\phi_k'\phi_i'\phi_j'\,ds + \frac{1}{2}\sum_{i=1}^{n}\sum_{j=1}^{n} q_iq_j\int_0^l \alpha_2 A\phi_i'\phi_j'\phi_k'\frac{V_H}{l}\,ds$$
$$+ \frac{1}{2}\sum_{i=1}^{n}\sum_{j=1}^{n}\sum_{m=1}^{n} q_iq_jq_m\int_0^l \alpha_4 A\phi_k'\phi_i'\phi_j'\phi_m'\,ds = \phi_k(0)f_t - \phi_k(l)f_b \tag{13}$$

By differentiating equation 10 with respect to time and using Ohm's law to represent the electrical damping as $\dot{Q} = \frac{V}{R}$,[11] we obtain

$$\sum_{i=1}^{n}\dot{q}_i e_{33}\frac{A}{l}\left[\phi_i(0) - \phi_i(l)\right] + \epsilon_{33}^S A\frac{\dot{V}}{l} - \frac{1}{6}\alpha_2 A\sum_{i=1}^{n}\sum_{j=1}^{n}\sum_{m=1}^{n}\left(\dot{q}_iq_jq_m + \dot{q}_mq_jq_i + \dot{q}_mq_iq_m\right)\int_0^l \phi_i'\phi_j'\phi_m'\,ds$$
$$- \frac{1}{2}\alpha_3 A\sum_{i=1}^{n}\sum_{j=1}^{n}\left(\dot{q}_iq_j + q_i\dot{q}_j\right)\int_0^l \phi_i'\phi_j'\,ds + \frac{V}{R} = 0 \tag{14}$$

3. LINEAR ANALYSIS

In this section, we investigate the response of the disk to a low excitation near the vibration frequency of the first thickness mode of disk. Because the excitation levels are relatively low, the corresponding strains in the body are not impacted by any nonlinearity in the system. When the modes are widely spaced, then the contribution of neighboring modes on the response of a particular mode is very low and hence, can be neglected. Removing the nonlinear parameters and considering only one mode, the governing equations of the first mode are given by

$$\ddot{q} + \omega_1^2 q + \left[\phi_1(0) - \phi_1(l)\right]\theta V + \dot{q}\left(2\zeta\omega_1 + R_r\phi_1^2|_{s=0} + R_r\phi_1^2|_{s=l}\right) - f_t\phi_1|_{s=0} + f_b(t-\tau)\phi_1|_{s=l} = 0 \tag{15a}$$

where ζ is damping ratio, and

$$-\theta\left[\phi_1(0) - \phi_1(l)\right]\dot{q} + C_p^{eq}\dot{V} + \frac{V}{R} = 0 \tag{15b}$$

where

$$\theta = -\frac{e_{33}A}{l}, \text{ and} \qquad C_p^{eq} = \frac{\epsilon_{33}^S A}{l} \tag{15c}$$

and the subscripts are dropped for the sake of convenience.

It is noted that the above equations are exactly same as those used by Shahab and Erturk[3] and Shahab et al.[4] Since the model is linear and the excitation is harmonic, the response is given by

$$V = V_0 e^{j\omega t} \qquad q = q_0 e^{j\omega t} \tag{16}$$

Downloaded From: https://www.spiedigitallibrary.org/conference-proceedings-of-spie on 7/17/2018
Terms of Use: https://www.spiedigitallibrary.org/terms-of-use

From equations 15a, 15b and 16, we determine the analytical expressions for voltage and modal displacement as:

$$V = \frac{j\omega\theta p_t \pi a_r^2 \left(\phi_1|_{s=0} - \chi e^{-j\omega\tau}\phi_1|_{s=l}\right)\left[\phi_1(0) - \phi_1(l)\right]}{\left[-\omega^2 + \omega_1^2 + j\omega\left(2\zeta\omega_1 + R_r\phi_1^2|_{s=0} + R_r\phi_1^2|_{s=l}\right)\right]\left(C_p^{eq} j\omega + \frac{1}{R}\right) + j\omega\theta^2\left(\phi_1(0) - \phi_1(l)\right)^2} \tag{17}$$

$$q = \frac{V}{j\omega\theta\left[\phi_1(0) - \phi_1(l)\right]}\left[C_p^{eq} j\omega + \frac{1}{R}\right] \tag{18}$$

By following a similar procedure as Shahab et al.,[4] the expression for electrical impedance is obtained as:

$$Z(\omega) = \left\{ j\omega\left[C_p^{eq} + \frac{\theta^2\left[\phi_1(L) - \phi_1(0)\right]^2}{\omega_1^2 - \omega^2 + j\omega\left[2\zeta\omega_1 + R_r\phi_1(0)^2 + R_r\phi_1(l)^2\right]}\right]\right\}^{-1} \tag{19}$$

4. NON-LINEAR ANALYSIS - PRIMARY THICKNESS RESONANCE

To study the effects of the system's nonlinearities as modeled above, we neglect the effect of the higher modes and write the nonlinear governing equations of first thickness mode as:

$$\ddot{q} + \omega_1^2 q + \dot{q}\left[2\zeta\omega_1 + R_r\phi_1^2|_{s=0} + R_r\phi_1^2|_{s=l}\right] + e_{33}A\frac{V}{l}\int_0^l \phi_1'\, ds + \alpha_3 A\frac{V}{l}q\int_0^l \phi_1'^2\, ds + \frac{1}{2}\alpha_1 A q^2\int_0^l \phi_1'^3\, ds + \frac{1}{2}\alpha_2 q^2 A\frac{V}{l}\int_0^l \phi_1'^3\, ds + \frac{1}{2}q^3\alpha_4 A\int_0^l \phi_1'^4, ds = \phi_1(0)f_t - \phi_1(l)f_b \tag{20a}$$

and

$$\dot{q}e_{33}\frac{A}{l}\left[\phi_1(0) - \phi_1(l)\right] + \epsilon_{33}^S A\frac{\dot{V}}{l} - \frac{1}{2}\alpha_2 A q^2\dot{q}\int_0^l \phi_1'^3\, ds - \alpha_3 A q\dot{q}\int_0^l \phi_1'^2\, ds + \frac{V}{R} = 0 \tag{20b}$$

Next, we use the Method of Multiple Scales[12] to determine the approximate solution of these equations and study the steady-state characteristics of the response. In physical systems, nonlinear terms are much smaller then the linear terms and hence are negligible at low excitations. In the present case, the quadratic and cubic terms in equations 20a and 20b are much smaller than linear acceleration term. So, we scale them to simulate the effects of the different terms and write

$$\ddot{q_1} + \omega_1^2 q_1 + 2\epsilon^2\mu\dot{q_1} + \epsilon\hat{\theta}q_2 + \epsilon\delta_1 q_1 q_2 + \epsilon\delta_2 q_1^2 + \epsilon^2\delta_3 q_1^2 q_2 + \epsilon^2\delta_4 q_1^3 = \frac{1}{2}\epsilon\omega\left(Fe^{j\omega t} + \overline{F}e^{-j\omega t}\right) \tag{21a}$$

$$-\hat{\theta}\dot{q}_1 + C_p^{eq}\dot{q}_2 - \epsilon^2\delta_3 q_1^2\dot{q}_1 - \epsilon\delta_1 q_1\dot{q}_1 + \epsilon^2\frac{q_2}{R} = 0 \tag{21b}$$

where

$$q_1 = q, \quad q_2 = V, \quad \mu = \frac{1}{2}\left[2\zeta\omega_1 + R_r\phi_1^2|_{s=0} + R_r\phi_1^2|_{s=l}\right], \quad F = j\rho_0 a^2\frac{Q}{4d_t}e^{-j\frac{\omega}{c_0}d_t}\left[\phi_1(0) - \chi\phi_1(l)e^{-j\omega\frac{l}{c_0}}\right],$$

$$\hat{\theta} = \left[\phi_1(l) - \phi_1(0)\right]\theta, \quad \delta_1 = \frac{A}{l}\alpha_3\int_0^l \phi'^2\, ds, \quad \delta_2 = \frac{1}{2}A\alpha_1\int_0^l \phi'^3\, ds, \quad \delta_3 = \frac{1}{2}\frac{A}{l}\alpha_2\int_0^l \phi'^3\, ds,$$

$$\delta_4 = \frac{3}{2}A\alpha_4\int_0^l \phi'^4\, ds \text{ and,} \tag{21c}$$

ϵ is a bookkeeping parameter that signifies the level to which the different terms in governing equations affect the response.[12,13]

To study the behavior of disk at primary resonance, we represent the excitation frequency as:

$$\omega = \omega_1 + \epsilon\sigma$$

Downloaded From: https://www.spiedigitallibrary.org/conference-proceedings-of-spie on 7/17/2018
Terms of Use: https://www.spiedigitallibrary.org/terms-of-use

where σ is a detuning parameter. Introducing three independent fast and slow time scales T_0, T_1 and T_2 defined by

$$T_n = \epsilon^n t \qquad n = 0, 1, 2$$

The solution of modal displacement $q(\equiv q_1)$ and voltage $V(\equiv q_2)$ can be then expressed as a series in ϵ of the form

$$q_1(t,\epsilon) = q_{10}(T_0,T_1,T_2) + \epsilon q_{11}(T_0,T_1,T_2) + \epsilon^2 q_{12}(T_0,T_1,T_2) + ... \tag{22a}$$

$$q_2(t,\epsilon) = q_{20}(T_0,T_1,T_2) + \epsilon q_{21}(T_0,T_1,T_2) + \epsilon^2 q_{22}(T_0,T_1,T_2) + ... \tag{22b}$$

Substituting the series expansions described in equations 22a and 22b into the governing equations 21a and 21b, and equating terms with equal power of ϵ, we obtain q_{10}, q_{11}, q_{12} and q_{20}, q_{21} and q_{22} depending on the extent of expansion. Elimination of the secular terms at highest expansion yields D_1A and D_2A. From the expressions for D_1A and D_2A, the modulation equations can be obtained from the chain rule as:

$$\dot{A} = \epsilon D_1 A + \epsilon^2 D_2 A \tag{23}$$

By representing of the complex amplitude in the polar form as, $A = \frac{1}{2}ae^{j\beta}$ and separating real, imaginary parts, we obtain the amplitude and phase modulation equations as:

$$\dot{a} = f_1(a,\gamma,\omega,\omega_1,F,\hat{\theta},C_p,\phi_1,\alpha_1,\alpha_2,\alpha_3,\alpha_4) \tag{24a}$$

$$\dot{\gamma} = f_2(a,\gamma,\omega,\omega_1,F,\hat{\theta},C_p,\phi_1,\alpha_1,\alpha_2,\alpha_3,\alpha_4) \tag{24b}$$

where $\gamma = \beta - \epsilon\sigma t$.

The steady-state amplitude and phase modulation equations are found by setting $\dot{a} = 0$ and $\dot{\gamma} = 0$ in equations 24a and 24b which are then used to find out steady-state amplitude a_0 and phase γ_0 for a given excitation. From the steady-state amplitude and phase of the modal displacement, we determine the voltage using the approximate solution.

5. RESULTS AND DISCUSSION

Next, we apply the above analysis to a PZT disk (PRYY+0547) that is made of a ferroelectric hard piezoelectric material, manufactured by Physik Instrumente (PI) GmbH & Co. KG.

5.1 Impedance Validation

The material properties of the disk - Young's modulus, Y_{33}, damping ratio, ζ, electromechanical coupling, θ, and equivalent capacitance, C_p, - can be identified by matching the impedance measurements in air provided by the manufacturer and are tabulated in Table 1. The plot in Fig. 2 show that electric impedance evaluated using identified parameters into equation (19) is in agreement with the impedance plot provided by the manufacturer. It is worth mentioning that the radiation resistance and reactance are very negligible in air, due to lower density and velocity of sound in the medium.

Parameter [units]	**Value**
Thickness, l [mm]	3.908
Radius, a [mm]	5
Young's modulus, Y_{33} [Gpa]	131.38
Capacitance, C_p^{eq} [pF]	119.77
Electromechanical Coupling, $\theta = -0.7e_{33}A/l$ [Cm^{-1}]	-0.2039
Damping ratio, $\zeta = 1/(2Q_m)$	1/2000

Table 1. Material and geometric properties of the disk used in the model.

Downloaded From: https://www.spiedigitallibrary.org/conference-proceedings-of-spie on 7/17/2018
Terms of Use: https://www.spiedigitallibrary.org/terms-of-use

The plots also show that the short and open circuit natural frequencies of the disk in air are 525.1 kHz and 552.4 kHz respectively. A slight deviation away from the resonant frequencies is noted. This is due to influence of a radial mode vibration harmonics near the first thickness mode natural frequency, which is not accounted for in the analysis.

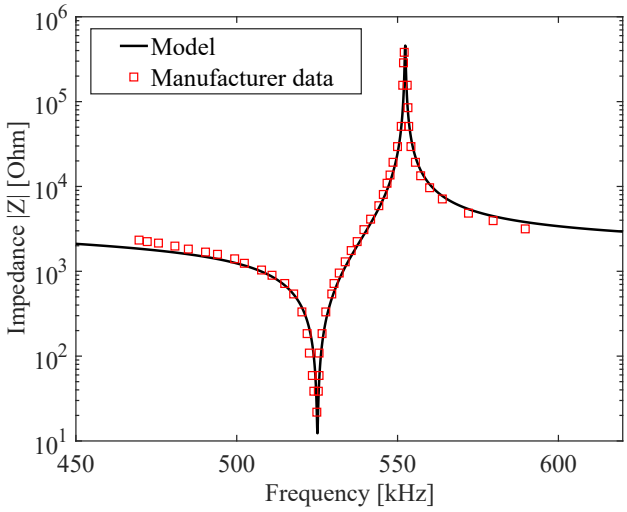

Figure 2. Comparison of electric impedance in air determined from the model with parameters listed in Table 1 to impedance measurements provided by the manufacturer.

5.2 Linear Response

The linear response, voltage and corresponding average power over a cycle generated by the disk when it is suspended in water is studied in this section. Using the material properties of the disk listed in Table 1, the linear response and corresponding voltage generated for an acoustic excitation for source strength $Q = 1\mu\text{m}^3/\text{s}$ is determined using equations 16 - 18. Figures 3(a) and 3(b) respectively present the steady-state amplitudes of displacement of the top surface, $u(s = 0)$ and voltage generated by the disk as a function of the excitation frequency for load resistance values between 500Ω and 10MΩ. Because the electrical load is purely resistive, average power in a cycle can be calculated using $P = \frac{1}{2R}V^2_{amplitude}$. Figure 3(c) shows the variation of average power for different load resistances. From Figs. 3(a) - 3(c), it is evident that the peak of the response gradually shifts from closed to open circuit natural frequency with the increase in load resistance, which is a typical characteristic of piezoelectric systems. From Fig. 3(c), it can also be concluded that the optimum load resistance for this particular disk is ≈ 1kΩ.

The linear response also shows an interesting unsymmetrical peak which can be explained by examining the amplitude of effective modal forcing on the disk. Figure 3(d) shows that the modal forcing amplitude gradually decreases from 420kHz to 570kHz which is why we have unsymmetrical peaks in figures 3(a) - 3(c). From the definition of modal forcing amplitude, this phenomenon can be accounted for the modal interaction, wave attenuation (χ) and phase difference between acoustic waves on the top and bottom surfaces of the disk.

5.3 Nonlinear Analysis

In this section, the nonlinear response of the disk when placed in water is discussed. Firstly, we validate the MMS by comparing the solution from steady-state amplitude and phase modulation equations for a low excitation, $Q = 1\mu\text{m}^3/\text{s}$ with the analytical expression for voltage and displacement in equations 17 and 18. Based on the plots presented in Fig. 4(a), we note that MMS accurately predicts the linear response for moderately low and very high load resistance.

Downloaded From: https://www.spiedigitallibrary.org/conference-proceedings-of-spie on 7/17/2018
Terms of Use: https://www.spiedigitallibrary.org/terms-of-use

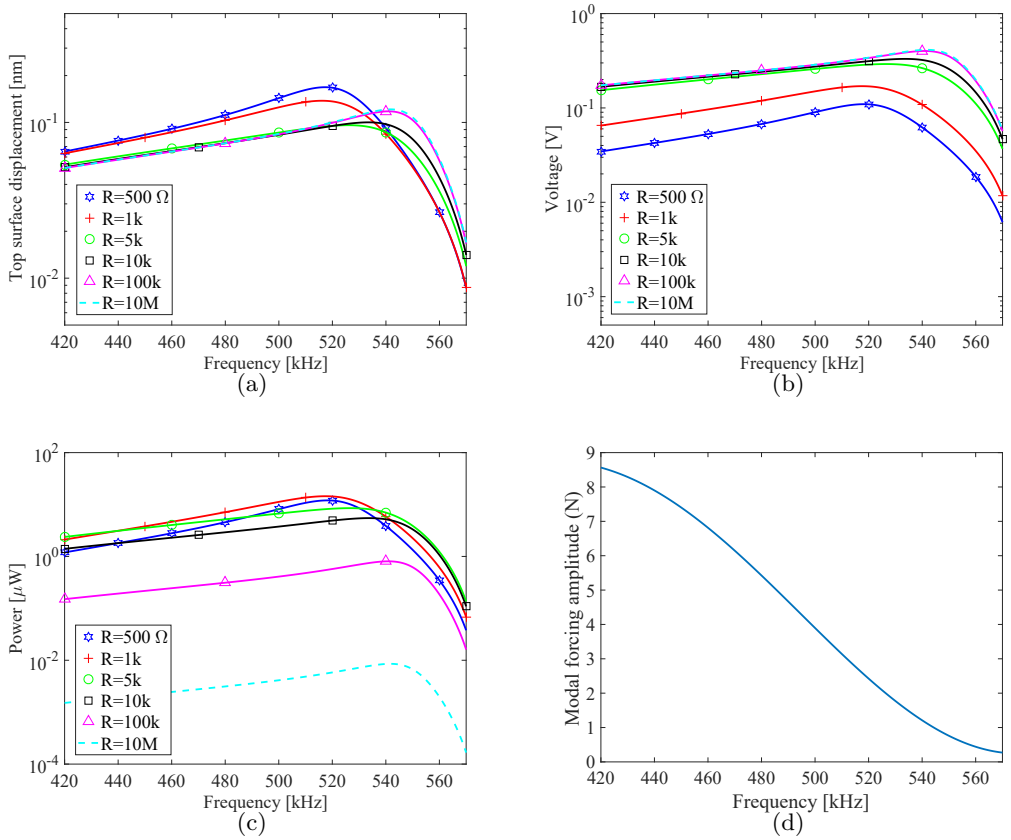

Figure 3. Figures showing (a) top surface displacement, (b) voltage generated by the disk, (c) Average power generated in a cycle and (d) modal forcing amplitude as a function of excitation frequency when $\rho_0 = 1000$ kg/m^3, $c_0 = 1500$ m/s, $R = 10^7$ Ohm, $\alpha_1 = 0$ Pa, $\alpha_2 = 0$ Cm^{-1}, $\alpha_3 = 0$ Cm^{-1}, $\alpha_4 = 0$ Pa and source strength, $Q = 1\mu$ m^3/s.

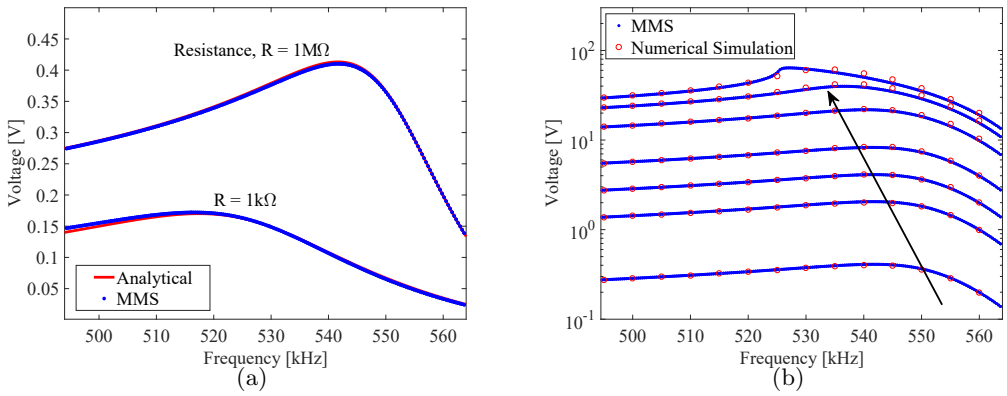

Figure 4. Figures showing (a) agreement between MMS and analytical solution for low source strength, $Q = 10^{-6}$ m^3/s (b) voltage generated by the disk as source strength is increased from 10^{-6} m^3/s to 10^{-4} m^3/s with $R = 10^7$ Ohm, $\alpha_1 = 5{\times}10^{15}$ Pa, $\alpha_2 = \frac{5}{6} \times 10^{11}$ Cm^{-1}, $\alpha_3 = \frac{25}{6} \times 10^5$ Cm^{-1} and $\alpha_4 = -\frac{25}{6} \times 10^{19}$ Pa ; in water $\left(\rho_0 = 1000\text{kg/m}^3,\ c_0 = 1500\text{m/s}\right)$. The direction of arrow indicates the increase in source strength.

Downloaded From: https://www.spiedigitallibrary.org/conference-proceedings-of-spie on 7/17/2018
Terms of Use: https://www.spiedigitallibrary.org/terms-of-use

Depending on the coefficients of cubic and quadratic nonlinearities in the governing equation, the frequency response for a nonlinear excitation exhibits hardening or softening behavior.[12] Based on the linear analysis and Fig. 3(d), we note that the forcing amplitude significantly drops for frequencies higher than natural frequency and hence a hardening behavior might not be appreciable to be noted. So, we choose α_1, α_2, α_3 and α_4 such that the system exhibits a softening type nonlinearity. Figure 4(b), presents the voltage generated as a function of forcing frequency when the source strength is increased from $Q = 1\mu\text{m}^3/s$ to $Q = 100\mu\text{m}^3/s$ for a load resistance $R = 10\text{M}\Omega$. It is observed that the peak gradually shifts from ≈ 552.4 kHz to ≈ 525.9 kHz as a consequence of softening nonlinearity.

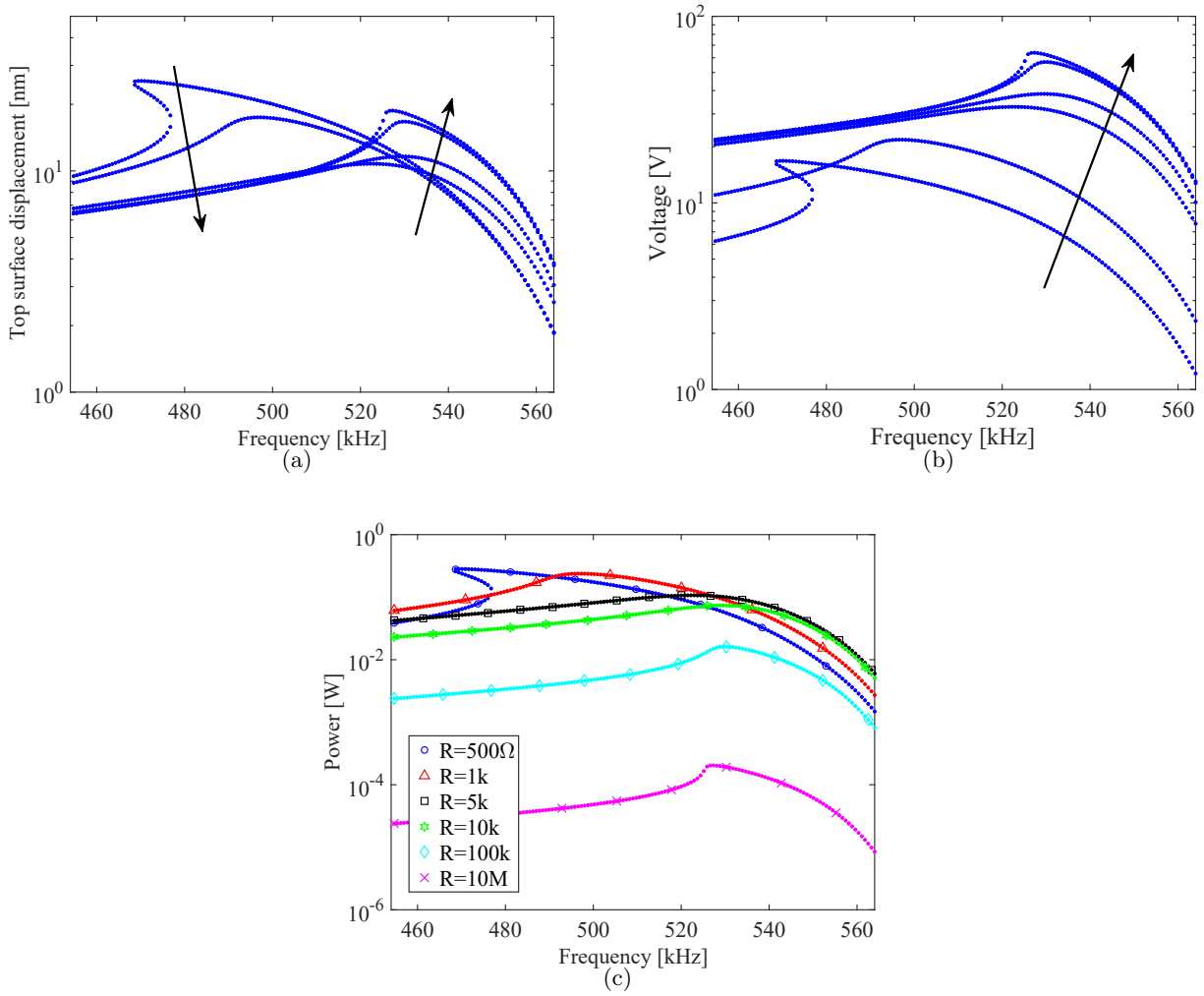

Figure 5. Figures showing (a) displacement of top surface (b) voltage generated and (c) average power in one cycle for source strength $Q = 100\mu\text{m}^3/\text{s}$ as the load resistance is increased from 100Ω to $10\text{M}\Omega$ with $\alpha_1 = 5\times10^{15}$ Pa, $\alpha_2 = \frac{5}{6}\times10^{11}$ Cm^{-1}, $\alpha_3 = \frac{25}{6}\times10^5$ Cm^{-1} and $\alpha_4 = -\frac{25}{6}\times10^{19}$ Pa in water $\left(\rho_0 = 1000\text{kg/m}^3,\ c_0 = 1500\text{m/s}\right)$. The direction of arrow indicates the increase in load resistance.

We further investigate the effect of nonlinear excitation on the response, voltage and average power generated by prescribing the source strength $Q = 100\mu\text{m}^3/\text{s}$ and changing the load resistance from 500Ω to $10\text{M}\Omega$. The results are presented in Figs. 5(a) - 5(c). From figure 5(a), the displacement of top surface near the short circuit natural frequency shows a very strong nonlinear behavior at low load resistances. This effect is gradually

Downloaded From: https://www.spiedigitallibrary.org/conference-proceedings-of-spie on 7/17/2018
Terms of Use: https://www.spiedigitallibrary.org/terms-of-use

reduced as load resistance is increased. On the contrary, near open circuit natural frequency, the nonlinear affect gradually increases as the load resistance is increased. From figure 5(b), the nonlinearity in the response is carried to the voltage generated as they are directly proportional for a given load resistance from equation **??**. It is interesting to note that, although the voltage generated at low load resistance is the lowest, it has the highest distortion in the peak and hence greater nonlinear influence. Figure 5(c) presents the average power generated over a cycle for different load resistances. By comparing the qualitative conclusions from Figs. 5(c) and 3(c), it is important to note that the optimum resistance which was $\approx$1kΩ for a linear excitation is shifted to $\approx$500Ω for a nonlinear excitation.

6. CONCLUSIONS

We tackled one of the major challenges in UAET, i.e., the nonlinear electro-elastic response of the receiver. We considered the nonlinear electro-elastic enthalpy used by Wagner and Hagedorn[6] and performed a theoretical analysis to assess the response of the PZT disk to acoustic excitation. For the particular dimensions and material of the disk used in this study, we illustrated how a possible softening nonlinearity could affect the response. Analytical results show that the optimum resistance in a nonlinear excitation is a function of forcing. They also suggest that in high amplitude excitations, the optimum resistance found using linear analysis can give poor energy transfer. In this study, we have neglected the attenuation of acoustic excitation and nonlinear effects due to the medium. In future work, the authors plan to include these effects and extend the study to a nonlinear electo-elastic receiver.

ACKNOWLEDGMENTS

This work was supported in part by the NSF Grant ECCS-1711139.

REFERENCES

1. M. G. Roes, J. L. Duarte, M. A. Hendrix, and E. A. Lomonova, "Acoustic energy transfer: A review," *IEEE Transactions on Industrial Electronics* **60**(1), pp. 242–248, 2013.
2. S. Shahab, S. Leadenham, F. Guillot, K. Sabra, and A. Erturk, "Ultrasound acoustic wave energy transfer and harvesting," in *Active and Passive Smart Structures and Integrated Systems 2014*, **9057**, p. 90570F, International Society for Optics and Photonics, 2014.
3. S. Shahab and A. Erturk, "Contactless ultrasonic energy transfer for wireless systems: acoustic-piezoelectric structure interaction modeling and performance enhancement," *Smart Materials and Structures* **23**(12), p. 125032, 2014.
4. S. Shahab, M. Gray, and A. Erturk, "Ultrasonic power transfer from a spherical acoustic wave source to a free-free piezoelectric receiver: Modeling and experiment," *Journal of Applied Physics* **117**(10), p. 104903, 2015.
5. S. Shahab, M. Gray, and A. Erturk, "An experimentally validated contactless acoustic energy transfer model with resistive-reactive electrical loading," in *Active and Passive Smart Structures and Integrated Systems 2015*, **9431**, p. 943105, International Society for Optics and Photonics, 2015.
6. U. Von Wagner and P. Hagedorn, "Piezo–beam systems subjected to weak electric field: experiments and modelling of non-linearities," *Journal of Sound and Vibration* **256**(5), pp. 861–872, 2002.
7. S. H. Crandall, *Dynamics of mechanical and electromechanical systems*, McGraw-Hill, 1968.
8. N. W. Hagood, W. H. Chung, and A. Von Flotow, "Modelling of piezoelectric actuator dynamics for active structural control," *Journal of Intelligent Material Systems and Structures* **1**(3), pp. 327–354, 1990.
9. H. F. Tiersten, *Linear Piezoelectric Plate Vibrations: Elements of the Linear Theory of Piezoelectricity and the Vibrations Piezoelectric Plates*, Springer, 2013.
10. J. L. Butler and C. H. Sherman, *Transducers and arrays for underwater sound*, Springer, 2016.
11. H. A. Sodano, *Macro-fiber composites for sensing, actuation and power generation.* PhD thesis, Virginia Tech, 2003.
12. A. H. Nayfeh and D. T. Mook, *Nonlinear oscillations*, John Wiley & Sons, 2008.
13. A. H. Nayfeh, *Introduction to perturbation techniques*, John Wiley & Sons, 2011.

Downloaded From: https://www.spiedigitallibrary.org/conference-proceedings-of-spie on 7/17/2018
Terms of Use: https://www.spiedigitallibrary.org/terms-of-use